JOURNAL OF GEOPHYSICAL RESEARCH, VOL. 100, NO. A11, PAGES 21,791–21,802, NOVEMBER 1, 1995

Location and characteristics of the reconnection X line deduced from low-altitude satellite and ground-based observations
1. Theory

M. Lockwood

Rutherford Appleton Laboratory, Chilton, Didcot, Oxfordshire, United Kingdom

Abstract. A method for estimating both the Alfvén speed and the field-aligned flow of the magnetosheath at the magnetopause reconnection site is presented. The method employs low-altitude cusp ion observations and requires the identification of a feature in the cusp ion spectra near the low-energy cutoff which will often be present for a low-latitude dayside reconnection site. The appearance of these features in data of limited temporal, energy, and pitch angle resolution is illustrated by using model calculations of cusp ion distribution functions. These are based on the theory of ion acceleration at the dayside magnetopause and allow for the effects on the spectrum of flight times of ions precipitating down newly opened field lines. In addition, the variation of the reconnection rate can be evaluated, and comparison with ground-based observations of the corresponding sequence of transient events allows the field-aligned distance from the ionosphere to the reconnection site to be estimated.

1. Introduction

The reconnection model of the magnetosphere predicts that plasma streams continuously across the magnetopause along open field lines which thread the boundary. This prediction has been confirmed by applications of the tangential stress balance test, both on the dayside [*Paschmann et al.*, 1979, 1986; *Sonnerup et al.*, 1981, 1990; *Paschmann*, 1984; *Johnstone et al.*, 1986] and on the boundary of the tail lobe [*Sanchez and Siscoe*, 1990; *Sanchez et al.*, 1990]. The open field line has a different orientation inside the magnetopause, in the low-latitude boundary layer (LLBL), from that in the magnetosheath. Between the two orientations is a region of field rotation, which is here referred to as the rotational discontinuity (RD). In practice the RD is likely to be structured; for example, the simplest form of Petschek reconnection predicts the field rotation to take place at the two shocks standing in the flow, and in general, more complex structure is expected [*Biernat et al.*, 1989]. We here refer to magnetosheath particles which have crossed the whole of the magnetopause current layer, and thus all of the structured RD, as being "injected." The distribution function of ions injected by flowing across the RD, along open field lines which are evolving away from the reconnection site, was predicted by *Cowley* [1982] to have a characteristic D shape. Note that these predictions depend on the field orientations on the two sides of the magnetopause current layer and not on the structure of the RD within it. The D-shaped distributions have recently been derived in numerical MHD and hybrid simulations [*Lin and Lee*, 1993] and have been observed in the dayside LLBL [*Gosling et al.*, 1990b; *Fuselier et al.*, 1991; *Smith and Rodgers*, 1991]. Furthermore, *Fuselier et al.* [1991] used the charge state of helium ions to identify and trace plasmas of magnetospheric and magnetosheath origins and showed that all populations, on both sides of the boundary, were as predicted by *Cowley* [1982]. *Smith and Rodgers* [1991] applied the stress balance test to show that the low-velocity cutoff of the D-shaped distribution function was the de Hoffmann-Teller velocity [*de Hoffmann and Teller*, 1950], as was also predicted by *Cowley* [1982]. The theory assumes that the RD is an ideal MHD one, in that there is acceleration but no heating of the ion gas on crossing the boundary, which may only be valid as a first-order approximation. In addition, the theory neglects ion scattering by assuming that pitch angle is conserved, both on transmission through and reflection off the current sheet: although this is clearly not valid for an individual particle, the above results show that, when dealing with large numbers of particles, scattering appears to have relatively minor effects on the overall distribution function. We here assume an ideal MHD RD to enable an estimation of the speed with which the field lines evolve over the boundary.

If the time elapsed since the field line in question was reconnected is lower than the time for it to evolve from the reconnection site to the magnetic cusp, it threads the dayside magnetopause, and the injected ions are accelerated on crossing the boundary and flow (along with sufficient electrons to maintain quasi-neutrality) toward the Earth, where they form the low-altitude "cleft" and "cusp" precipitations and contribute lower-energy ions to the "mantle" precipitation. However, after the field line has convected through the magnetic cusp, the injected ions are decelerated but still flow superthermally in the antisunward direction in the magnetospheric mantle [*Hill*, 1979; *Cowley et al.*, 1991]. Note therefore that although this high-altitude mantle, antisunward of the region around the magnetic cusp, is threaded by the same field lines as the region of low-altitude

Paper number 95JA01340.
0148-0227/95/95JA-01340$05.00

precipitation, which is also termed mantle, very little of the latter precipitation arises from the population in the magnetospheric mantle: by the time that the few Earthward-directed ions in the high-altitude mantle reach the ionosphere, the field line has convected into the low-altitude precipitation region termed "polar cap," where ions from the high-altitude mantle contribute to a low-density, low-energy (in the Earth's frame of reference) precipitation. The origin of low-altitude mantle precipitation was demonstrated by *Onsager et al.* [1993]. Their Figure 1 shows where ions of energy 32 eV and 30 keV must be injected in order for them to be detected at two latitudes in the low-altitude mantle region. The 32-eV ions come from the vicinity of the magnetic cusp. The higher-energy ions (30 keV) would come from higher latitudes, but Figure 2 of *Onsager et al.* [1993] shows that the flux of such particles is negligible. Therefore the low-altitude mantle population comes from the dayside (at energies below about 32 eV) or the immediate vicinity of the magnetic cusp, with negligible fluxes from higher latitudes in the high-altitude mantle.

As a result of these combined effects, precipitation of magnetosheathlike plasma is seen at low altitudes in a relatively narrow band of latitudes and evolves in nature as the newly opened field line evolves antisunward into the tail lobe [*Cowley et al.*, 1991; *Lockwood et al.*, 1993a]. At its most dense, the precipitation is referred to as "cusp" [*Heikkila and Winningham*, 1971; *Frank*, 1971; *Newell and Meng*, 1988]. There is much evidence that this cusp precipitation is indeed on newly opened field lines as the reconnection model predicts, as has recently been reviewed by *Lockwood and Smith* [1994].

The location of the reconnection site is not known in detail. For southward interplanetary magnetic field (IMF), magnetopause and cusp observations indicate that the reconnection which opens field lines often takes place at relatively low latitudes. For example, the accelerated ion flows in both hemispheres are always directed away from low latitudes [*Cowley*, 1982; *Gosling et al.*, 1990a]. This phenomenon contrasts with situations where the sheath field points northward, giving accelerated flows away from a high-latitude (lobe) reconnection site [*Gosling et al.*, 1991]; such flows are therefore equatorward when viewed in the same hemisphere as the reconnection site [*Paschmann et al.*, 1990]. (Note that, unlike the reconnection at latitudes below the magnetic cusp, this lobe reconnection does not produce new open flux but, rather, reconfigures existing open flux.) The sense of the dawn-dusk component of the accelerated flow, relative to the sense of the same component of the IMF, is also consistent with a low-latitude site [*Gosling et al.*, 1990]. In addition, the polarity of the boundary normal field, as derived from stress balance tests, reverses sense across low latitudes [*Paschmann*, 1984]. *Onsager and Fuselier* [1994] have compared the recently injected Cowley D distribution seen in the LLBL with the one that was seen simultaneously but was injected earlier and has mirrored at low altitudes and returned to the satellite. In this way they defined the reconnection site to be within 6 R_E of the subsolar point for both northward and southward IMF. A similar technique was applied to mid-altitude cusp observations by *Phillips et al.* [1993] and a similar result obtained, at least for observations close to the open/closed boundary, for which the cut-off of the D distributions are at higher energies and more clearly defined. *Reiff et al.* [1977] estimated a low-latitude reconnection site from the dispersion and convection of cusp ions at low altitudes, and *Onsager et al.* [1993] modeled low-altitude cusp observations, using the open model with a subsolar reconnection site. However, the uncertainties in determination of the X line location from low- and mid-altitude cusp observations are large. Some cases, like that discussed by *Phillips et al.* [1993], are for times when the IMF is closely aligned with the -Z (GSM) direction, for which both "component" and "antiparallel" models of reconnection predict that the reconnection site will be close to the subsolar point [*Crooker*, 1979]. Global MHD models of the magnetosphere have shown that reconnection rate changes with IMF orientation, in close agreement with observations, but that the reconnection site does not move as predicted by the antiparallel hypothesis [*Fedder et al.*, 1991]. The reconnection which opens field lines during southward IMF (i.e., between closed field lines and the sheath field) must take place between the magnetic cusps, and the above evidence suggests that it often takes place at relatively low latitudes. However, it is not yet known how confined to low latitudes such reconnection may be, and any dependence of the location of the reconnection site on the orientation of the IMF is not yet clear.

Figure 1 shows schematically the dayside magnetosphere in the open magnetosphere model for southward IMF conditions with a low-latitude reconnection site. A newly opened field line is shown in four positions (labeled 1-4) as it evolves away from the reconnection site, *X*, under the influence of the magnetic curvature force ("tension") and the magnetosheath flow. The points P_n are where the field line

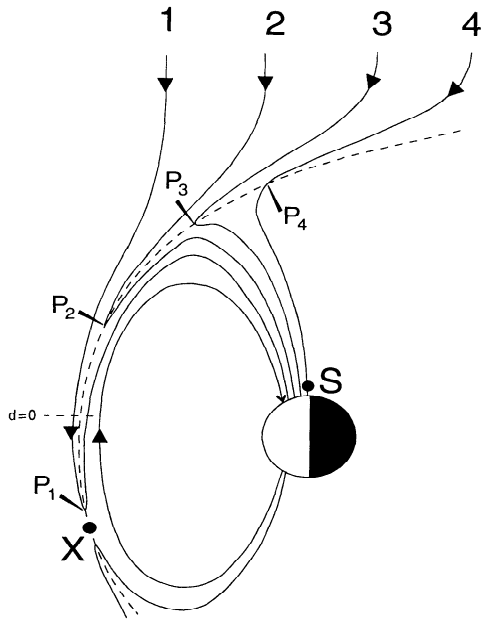

Figure 1. The evolution of a newly opened field line from a dayside magnetopause X line, *X*, into the tail lobe. Each field line evolves through the positions marked *n*, in which it threads the magnetopause at point P_n. Ions injected across the magnetopause at P_n are spread along the corresponding dashed line in Figure 2. The satellite, *S*, is shown making observations on a field line in position 4, in the northern hemisphere topside ionosphere, a field-aligned distance d_o from the X line.

(in position n) threads the magnetopause. Each newly opened field line executes this sequence, and ions stream across the boundary at all P_n. The satellite S is shown in the northern hemisphere topside ionosphere, making observations on a newly opened field line which is in the position labeled 4. The diagram shows three earlier positions of that newly opened field line as it evolves from the X line toward the tail lobe: Position 1 is shortly after the field line was reconnected at X; in position 2 it threads the magnetopause at higher latitudes on the dayside (P_2); in position 3 the field line is approaching the magnetic cusp; and in position 4 it is becoming appended to the tail lobe. In Figure 1, X is placed away from the geomagnetic equator to stress that the field-aligned distance between X and the ionosphere at the altitude of S, d_o, is variable. We may expect d_o to vary with the Earth's dipole tilt (i.e., with season and time of day) as well as with the IMF orientation (because of magnetospheric erosion by reconnection) and the solar wind dynamic pressure (because of magnetospheric compression).

Both magnetopause observations and recent auroral and flow measurements in the cusp/cleft ionosphere suggest that the reconnection may sometimes or often take place in a series of pulses, with slower or zero reconnection taking place between the pulses (see reviews by *Lockwood*, [1994, 1995a]). The possible reasons for this behavior are not yet known, but understanding would be greatly enhanced if the exact location of, and the conditions at, the reconnection site were known. This paper presents a theory enabling such information to be derived from observations of the cusp by low-altitude satellites and ground-based radars. A companion paper [*Lockwood et al.*, this issue] describes the application of this theory to observations by the DMSP-F10 satellite and the European Incoherent Scatter (EISCAT) radars.

2. Time-of-Flight Effects

The velocity filter effect of injected cusp ions was first discussed by *Rosenbauer et al.* [1975], *Shelley et al.* [1976], *Reiff et al.* [1977], and *Hill and Reiff* [1977]. Ions of different field aligned velocity, injected simultaneously across the magnetopause onto any one field line, have different flight times along that field line. Hence they have different arrival times in the ionosphere and, as the field line is convecting, are spatially dispersed along the locus of the field line. In other words, the trajectories of ions precipitating down field lines are only field aligned if there is no convection and the magnetosphere is stagnant [*Lockwood and Smith*, 1993]. The magnetosphere is generally not stagnant, and as a result, the angle that an ion trajectory makes with the field line depends on its energy. A spectrum of ion energies seen simultaneously at low altitudes therefore reveals a spread of injection locations.

Figure 2 illustrates some important consequences of this velocity filter effect. Consider a low-altitude satellite, S, which is moving equatorward while convection is poleward (but at a speed less than the satellite speed; see discussion by *Lockwood and Smith* [1994]). It is useful to consider components of velocities which are normal to the open-closed field line boundary (OCB), positive to the poleward side of the OCB, and measured in the rest frame of the OCB: V_S is this component of the satellite velocity, and V_c is this component of the convection velocity. We here consider an example with $V_c > 0$, $V_s < 0$, and $|V_c| << |V_s|$. This situation is chosen

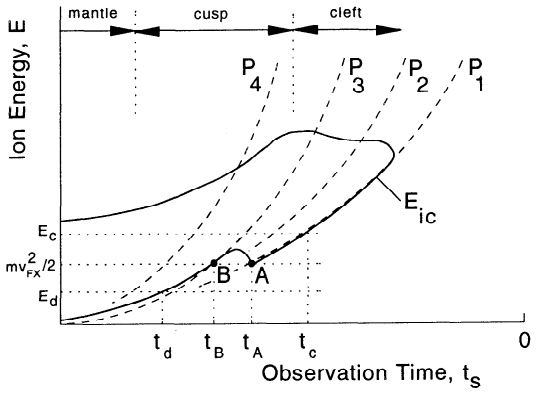

Figure 2. Schematic of cusp ion precipitation observed by an equatorward moving satellite for poleward convection (southward IMF). The lower and upper solid lines show the minimum and maximum detectable energies, E_{ic} and E_{max}, respectively, as a function of observation time t_s. The dashed lines connect ions injected at a point P_n (see Figure 1) on the magnetopause which each newly opened field line reaches a time t_n after it is reconnected, where $t_4 > t_3 > t_2 > t_1$. Also shown are typical boundaries of the cleft, cusp, and mantle regions defined from the spectral characteristics at any one t_s. In this Figure, the X line is close to P_1 from which the field lines evolve along the magnetopause at a de Hoffmann-Teller velocity of V_{fX}.

as it applies to the observations described in the companion paper [*Lockwood et al.*, this issue]. Figure 2 shows schematically the variation of the maximum and minimum energies of detectable flux of magnetosheathlike ions, seen by S as a function of observing time t_s. At any one t_s, the satellite sees ions with a range of energies and hence with a range of field aligned speeds and flight times from the magnetopause: because the field line (onto which these ions are frozen) is convecting, this corresponds to a range of injection locations and times [*Lockwood and Smith*, 1993; *Onsager et al.*, 1993]. It is useful to here consider where the satellite will detect the dispersed spectrum of field-aligned ions injected at any one point P_n on the magnetopause, which each newly opened field line reaches a time t_n after it is opened. The higher-energy ions of this spectrum at the magnetopause have lower flight times and, because of the poleward convection of that field line, are seen at lower latitudes in the ionosphere (and thus at higher t_s for this example of an equatorward moving satellite). For scatter-free adiabatic motion, all ions are seen by the satellite with the same energy of field-aligned motion, E_n, and (by Liouville's theorem) distribution function, f, as they had at P_n. The energy and observation time are related by the time-of-flight equation for zero pitch angle ions:

$$d_n(m/2E_n)^{1/2} = t_s - (t_o + t_n), \quad (1)$$

where m is the ion mass, d_n is the distance along the field line from P_n to the altitude of the satellite, and t_o is the time that the field line (observed by the satellite at time t_s) was opened by reconnection. If we define $t_s = 0$ to be when the satellite crosses the OCB (where $t_o = t_s$), the satellite has moved a distance $V_s t_s$ poleward in the OCB rest frame to the point of observation by the time t_s. At this point and time, the satellite will observe a field line which was opened at an earlier time, t_o, and which will have moved at constant speed

V_c (for a steady reconnection rate) away from the OCB in its own rest frame in the interim period of $(t_s - t_o)$. The distance moved poleward by the field line to the observation point, in the OCB rest frame, is thus equal to $V_c(t_s - t_o)$, and this will equal the distance of the satellite poleward of the OCB, $V_s t_s$. Substituting $(t_s - t_o) = (V_s/V_c)t_s$ into (1) yields

$$E_n = (m/2)\, d_n^2/\{(V_s t_s/V_c) - t_n\}^2 \qquad (2)$$

In Figure 2, dashed lines are defined by equation (2) and join ions sharing the same injection location. Four such lines are shown, for injection points P_1 to P_4, for which $t_4 > t_3 > t_2 > t_1$. Also shown in this Figure are typical boundaries of the three ionospheric regions of magnetosheathlike particle precipitation, termed cleft, cusp, and mantle. These are defined for each t_s by the density and spectra of the electron and ion precipitation, often by using the classifications devised by *Newell and Meng* [1988] and *Newell et al.* [1991]. Notice that any one injection point will usually contribute ions to more than one of these regions and that the ion spectrum seen by the satellite at any one time, t_s, is an ensemble, with different energies coming from different injection locations [*Lockwood and Smith*, 1993]. Indeed, equation (2) shows that any one point on the magnetopause, P_n, can only contribute one ion energy to the spectrum seen at any one observation time t_s [*Onsager*, 1994].

Notice that no convection in the Earth's frame is required to cause this so-called velocity filter effect. As pointed out by *Lockwood and Smith* [1989] and *Lockwood et al.* [1993b], V_c in the above equations is in the OCB rest frame and could arise from zero convection in the Earth's frame if the OCB is eroding equatorward (at speed V_c).

3. Injected Ion Distributions in the LLBL

The theory of *Cowley* [1982] predicts that the injected plasma in the open LLBL (also called the "reconnection layer") will show a characteristic D-shaped ion velocity distribution, as has been confirmed by recent observations (see introduction). Two key parameters of this truncated drifting Maxwellian distribution are the field-aligned velocities of the distribution function peak, V_p, and the low-velocity cutoff, V_{min}. Figure 3a shows the general situation at the rotational discontinuity formed by the newly-opened field lines where they thread the magnetopause at a point P_n. The Z axis points along the magnetopause in the direction of motion of the newly opened field lines, and the X axis is the outward normal to the boundary. The field line makes angles ϕ and θ with the magnetopause on its magnetosheath and magnetospheric sides respectively. These angles increase with the distance d from X to P_n, as the field line straightens. Figure 3a is in the de Hoffmann Teller (dHT) frame of reference in which the newly opened field lines are at rest. In the Earth's frame of reference both the dHT frame and the field lines move along the magnetopause in the Z direction at speed V_f (which is typically 100-300 km s^{-1}, corresponding to a field-perpendicular convection velocity of about 10-30 km s^{-1} on the Earthward side of the RD in the (open) LLBL [*Aggson et al.*, 1983; *Sonnerup et al.*, 1990]).

Cowley's [1982] predictions were made by using a geometric construction like that shown in Figure 3b. This is a velocity space plot in the Earth's frame (V_x', V_z') and in the dHT (V_x, V_z) frame. We here consider the simpler symmetric

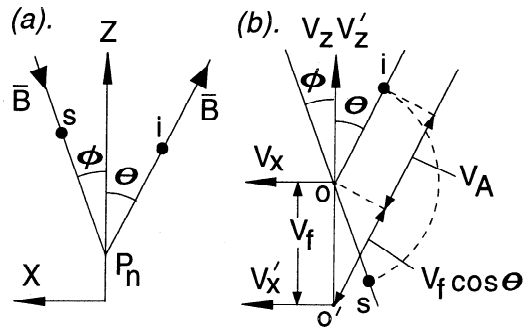

Figure 3. (a) The rotational discontinuity (RD) formed by a newly opened field line at P_n which evolves along the magnetopause in the Z direction at speed V_f in the Earth's frame of reference. The X direction is the outward normal to the boundary. (b) A velocity space plot showing field-aligned bulk flow at the Alfvén speed, V_A, in the de Hoffmann-Teller frame (V_x,V_z with origin at O) both into the RD in the magnetosheath (at s) and away from the RD in the magnetosphere (at i). This geometric construction allows the calculation of the minimum and bulk flow field-aligned speed of injected particles in the Earth's frame (V_x',V_z' with origin at O'). (Adapted from *Cowley* [1982]).

case in which the Alfvén speed is the same on the two sides of the boundary. The theory of a time-stationary, one-dimensional ideal MHD RD reveals that the plasma will flow through the RD at the local Alfvén speed, V_A, in the dHT frame [*Hudson*, 1970]. Sheath ions approaching the magnetopause have $V_x < 0$ and $V_z < 0$ (s in Figure 3b), but once injected they have $V_x < 0$ but $V_z > 0$ (i in Figure 3b). About this bulk flow speed is the thermal spread, and only ions with $V_x < 0$ will cross the magnetopause. The minimum injected field-aligned velocity in the dHT frame is zero, and Figure 3b shows that this gives a minimum field-aligned velocity in the Earth's frame of

$$V_{min} = V_f \cos\theta \qquad (3)$$

and the field-aligned velocity of the distribution function peak in the Earth's frame is

$$V_p = V_f \cos\theta + V_A\,. \qquad (4)$$

Because the distribution is truncated, V_p is slightly lower than the field aligned bulk flow speed.

Cowley and Owen [1989] have noted that the field line velocity V_f is such that the sheath flow in the Earth's frame results in the field-aligned inflow speed in the dHT frame being V_A, i.e., by a frame transformation from the dHT to the Earth's frame,

$$V_f = V_{sh} + V_A \cos\phi\,, \qquad (5)$$

where the velocity V_{sh} is the component of the tangential magnetosheath flow along the boundary which lies in the plane of the magnetosheath field. Thus in the Earth's frame there is a minimum field-aligned ion energy of the injected population of

$$E_{min} = m\, V_{min}^2/2 = m([V_{sh}+V_A \cos\phi] \cos\theta)^2/2\,. \qquad (6)$$

Lockwood and Smith [1994] employed this formulation to show that E_{min} first rises as the field line accelerates away from the X line (V_f increases) but then falls to zero as θ increases to 90° near the magnetic cusp.

Figure 4 shows schematically the field-parallel distribution functions injected at the positions P_n shown in Figure 1, and at times $(t_n + t_o)$, i.e., at elapsed times since reconnection of t_n. They have the truncated, drifting maxwellian shape of the Cowley D distributions. Near the X line (position 1) the angle θ is sufficiently close to zero that cos θ can be taken as unity and the distribution cutoff velocity, V_{min}, is equal to V_{fX}, the dHT velocity in the immediate vicinity of the X line where the field-aligned velocity of the peak of the injected distribution is V_{p1}. The other 3 injection locations shown in Figure 1 are further removed from the X line where the magnetosheath temperature and density are both smaller [*Spreiter et al.*, 1966]. *Lockwood and Smith* [1994] have shown that both V_{min} and V_p increase as the field line accelerates away from the X line, and these factors are reflected in Figure 4 for the distribution injected when the field line is in position 2. However, as the field line approaches the magnetic cusp, it straightens, and both velocities decrease again. The position P_3 in Figures 1, 2, and 4 is a special one, in that it is where V_{min} returns to its value at the X line, V_{fX}. By the time the field line has evolved to position 4, the ion acceleration on crossing the magnetopause has turned to a deceleration, and V_{min} falls to zero.

4. Spectrum of Ions Seen at Low Altitudes

Each newly opened field line undergoes the evolution shown in Figure 1, and hence each has the sequence of distributions shown in Figure 4 injected onto it. We are only concerned with this near field-parallel part of the injected distribution which is seen at low altitudes, all other pitch angles being mirrored in the converging magnetic field lines before reaching the satellite S. Prior to a field line being opened at time t_o, no ions were injected. For ions injected at the X line, t_n has a minimum value of zero which by equation (1) yields a minimum of the ion energy we call the "lower cutoff" energy, E_{ic}. Ions injected in the immediate vicinity of the X line at P_1 are dispersed along the line marked P_1 in Figure 2, given by equation (1) for d_n equal to the field-aligned distance between the ionosphere (at the altitude of the satellite) and the X line, d_o (we consider a P_1 so close to X that $d_1 \approx d_o$). However, because there is a minimum energy injected at the X line (corresponding to $V_{min} = V_{fX}$), particles cannot be seen along this dashed line below the point A, at an energy of $(mV_{fX}^2/2)$. As a result, no ions are seen from the X line (by the equatorward moving S) before the time t_A, the value of t_s at the point A. Equation (1) (with $t_n = 0$ and $d_n = d_o$) shows that E_{ic} will rise as the satellite moves equatorward toward the OCB as the elapsed time since reconnection $(t_s - t_o)$ decreases.

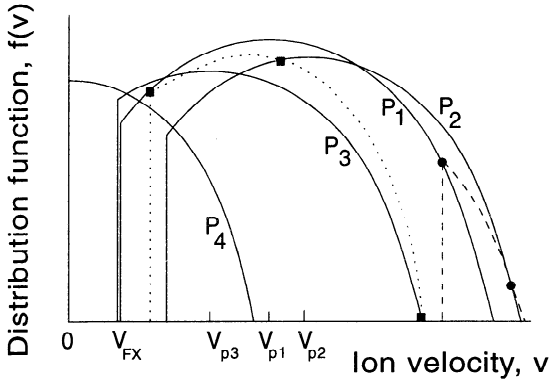

Figure 4. Field parallel segments of the Cowley D ion distribution functions in the open LLBL, injected across the magnetopause at P_n in Figure 1. These distributions are shown as $f(v)$ on log-linear axes and are dispersed along the corresponding dashed lines in Figure 2. The dashed line joining the solid circles is the spectrum seen at low altitudes at a time t_s, such that the satellite is in the region classed as cleft. the dotted line joining the squares is an example of that seen when S is in the "cusp" region.

Figure 2, like Figure 4, is drawn such that V_{min} for the point P_3 is the same as at the X line (V_{fX}). The spectrum injected at P_3 is spread along the line marked 3 in Figure 2 down to the point B (encountered by the satellite at $t_s = t_B$). At times between t_A and t_B, the lowest-energy ions come from points like P_2 (Figure 1), for which V_{min} is higher.

In addition to these changes in the cutoff ion energy, the shape of the spectrum seen at low altitudes will evolve with $(t_s - t_o)$ because of a combination of the evolution of the injected spectrum and time-of-flight effects. This is demonstrated by Figure 4. For example, high-energy ions injected at P_2 will arrive at the satellite simultaneously with ions of energy E_{ic} from P_1. The solid circles in Figure 4 mark the parts of the distributions from P_1 and P_2 which arrive simultaneously at S, at a t_s which is comparatively late in the pass (when $(t_s - t_o)$ is low and S is in the region classed as cleft in Figure 2). The dashed line joining them is the rest of the spectrum observed at that time. The largest f observed is from close to the X line, and is at the velocity of the time-of-flight cutoff; in other words, the peak f is $f(E_{ic})$ at this t_s. The solid squares are the parts of the distributions injected at P_1, P_2 and P_3 seen at an earlier t_s (when $(t_s - t_o)$ is larger and S is in the cusp region in Figure 2), and the dotted line shows the full distribution observed at that time. Note that at this earlier t_s, the peak f is not $f(E_{ic})$ and comes from the midlatitude magnetopause (like point P_2) rather than the X line. Comparison of these two spectra shows that the peak f observed at any one t_s does not bear a fixed relationship with the cutoff and hence cannot be used to define the cutoff. The only exception to this is nearer the open-closed boundary where the peak f and the cutoff are at the same (larger) velocity.

5. Analytic Calculations of Cusp Ion Distribution Functions

This section presents some analytic calculations of the spectrum of ions seen at low altitudes. These not only confirm the schematic shown in Figure 4, but also reveal new features which section 7 shows to have important applications for investigation of the reconnection site. These calculations are an extension of those presented by *Lockwood and Smith* [1994] and are based on gasdynamic model predictions of the variations of magnetosheath density, temperature, and flow along the magnetopause along with input variations of the RD angles θ and ϕ and the field-aligned distance from the magnetopause to the satellite, d_n. These input parameters are specified by polynomial fits to model results as a function of distance, d, from the stagnation

point at the nose of the magnetosphere, and are shown in Figures 5 and 6. The gasdynamic model is that of *Spreiter et al.* [1966] for a solar wind Mach number of 8, a velocity of 400 km s^{-1}, a temperature of 2×10^5 K and a dynamic pressure which places the subsolar magnetopause at $X = 10$ R_E. This yields the along-boundary variations with d shown in Figure 5 of the sheath temperature T_{sh}, velocity V_{sh}, and density N_{sh} (expressed as a ratio of the undisturbed solar wind value, N_{sw}). Note that in general, the gasdynamic approximation breaks down close to the magnetopause, and in particular, plasma densities may be reduced and the ion temperature become anisotropic in a plasma depletion layer if draped and compressed field gives sufficient Maxwell pressure. However, no such effects have been included here. Figure 6 also shows the time t_n that a newly opened field line takes to convect the distance to P_n from the reconnection site, taken here to be at the nose of the magnetosphere so this distance is equal to d. This is computed from the variation of V_f with d, using equation (5) and a constant Alfvén speed of $V_A = 165$ km s^{-1}, in the same way as employed by *Lockwood and Smith* [1994]. Note that V_{sh} in (5) is the component of the magnetosheath flow tangential to the boundary and in the plane of the magnetosheath field. For simplicity we here take the sheath field to be aligned so that there is no flow perpendicular to this plane.

Equation (1) can be used to compute which one ion energy, E_n, will be seen from an injection point, P_n (reached by the newly opened field line a time t_n after reconnection and at a field-aligned distance d_n from the satellite altitude) for a given time elapsed since reconnection (t_s - t_o). The results are shown by the solid lines in Figure 7 as a function of d and for various (t_s - t_o). At every d we can also compute the distribution function of particles injected into the LLBL from the values of V_{min}, V_p (from equations (3), (4) and (5)) by considering a Maxwellian centered on V_p which is truncated at V_{min} (the field-parallel segment of the Cowley D distribution). The fraction of ions incident on the magnetopause which are injected (the "transmission factor", t) is taken to be independent of d, and it is assumed that there is no heating on crossing the boundary, so that the field-parallel temperature of the Cowley D, T, is the same as the T_{sh} at that d. Figure 7 shows the variation of the energies E_{min} and E_p

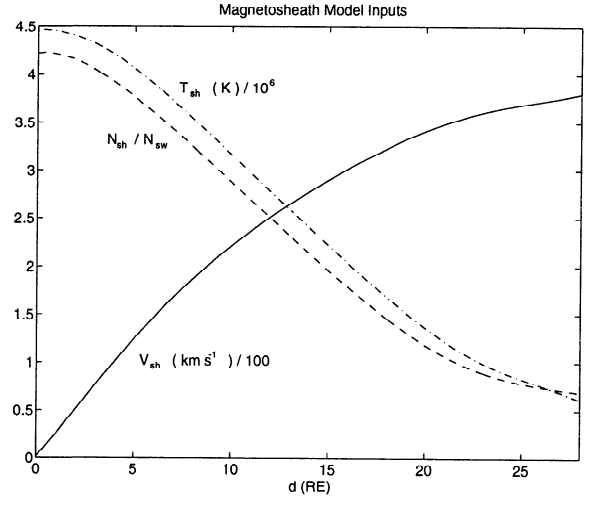

Figure 5. Variations of model magnetosheath inputs with distance from the nose of the magnetosphere, d, based on the gas dynamic calculations of *Spreiter et al.* [1966]. The solid line is the flow along the boundary, V_{sh} (in kilometers per second), divided by 100; the dashed line is the sheath density N_{sh}, as a ratio of the density of the undisturbed solar wind (N_{sw}); and the dot-dashed line is the sheath ion temperature, T_{sh} (in degrees Kelvin), divided by 10^6.

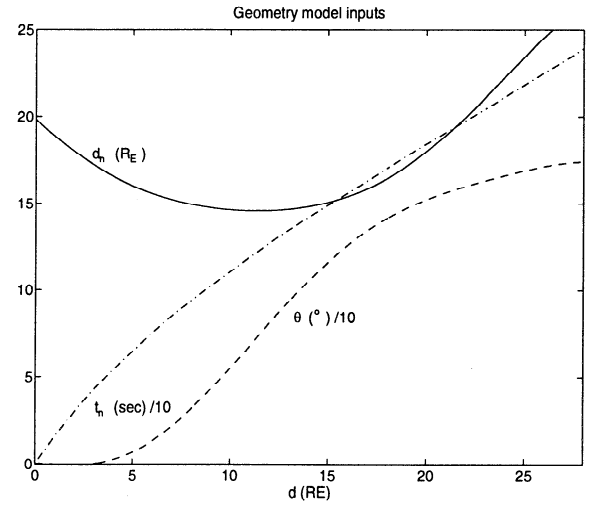

Figure 6. Variations of model parameters with distance d from the nose of the magnetosphere for an X line at $d = 0$. The solid line is the field-aligned distance d_n from the injection point P_n to the satellite (in units of Earth radii); the dot-dashed line is t_n (in seconds)/20, where t_n is the time for the field line to convect from the X line to P_n; and the dashed line is θ (in degrees)/10, where θ is defined by Figure 3a. Here, d_n and θ are assumed inputs into the model, whereas t_n is computed by the model (see text for details).

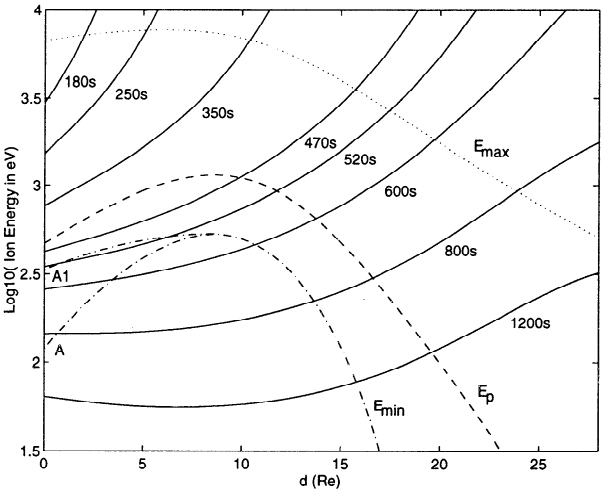

Figure 7. The ion energy E_n received by the satellite from the magnetopause point P_n, shown (by solid lines) as a function of the distance d of P_n from the nose of the magnetosphere and for various elapsed times since reconnection (t_s-t_o). The dot-dashed, dashed, and dotted lines are, respectively, the minimum energy (E_{min}), the energy of peak distribution function (E_p), and the maximum energy of detectable ion flux (E_{max}) injected at P_n, all as a function of d. The lower dot-dashed (E_{min}) trace at low d is the minimum ion energy injected at each P_n, whereas the upper one is the minimum ion energy which can reach the ionosphere from there without a second encounter (and hence further acceleration) at the magnetopause.

corresponding to V_{min} and V_p as dot-dashed and dashed lines, respectively. Note the rise and fall with d, reflecting the acceleration and subsequent straightening of the newly opened field lines, as discussed by *Lockwood and Smith* [1994]. It also shows the maximum detectable energy, E_{max}, here crudely computed by assuming that the detector can see f down to 10^{-4} times the peak value injected at the nose of the magnetosphere, f_p. The value of E_n for $d = 0$ is E_{ic} and falls with $(t_s - t_o)$ until it reaches E_{min} at $(t_s - t_o)$ greater than about 800 s, after which the only ions observed are from the near magnetic cusp at a d between about 15 and 24 R_E (along the solid line between E_{min} and E_{max}). Thus the point A in Figure 2 is near $(t_s - t_o) = 800$ s in this case. Note that for mid-range values of $(t_s - t_o)$, ions come from the whole dayside magnetopause (e.g., at $(t_s - t_o) = 470$ s, ions come from d between zero and about 16 R_E).

The dot-dashed line (E_{min}) in Figure 7 can be seen to bifurcate at low d. This is because the lowest energy ions injected near the X line will not precipitate adiabatically into the ionosphere when the field line is accelerating (M. P. Freeman, private communication, 1995); instead, they will return to the magnetopause and be accelerated, either in being transmitted through it, or in being reflected by it. This is because the field-aligned distance between an ion and the magnetopause increases at a rate $[V_{fi} \cos \theta_i + V_i - V_f \cos \theta]$ (where the subscript i refers to values at the injection point where the ion crossed the boundary at speed V_i in the de Hoffman-Teller frame), and hence this distance can decrease if $V_f \cos \theta > V_{fi} \cos \theta_i$. In Figure 7, the lower E_{min} trace at low d refers to the minimum injected energy, whereas the upper curve is the minimum energy which reaches the ionosphere without encountering the magnetopause for a second time. Thus allowing for this effect, A in figure 2 refers to A1 in figure 7. In this paper, we simplify this effect by saying that all ions which do encounter the magnetopause for a second time are lost to the magnetosheath. The intersection of the solid lines for E_n with E_{min}, E_p, and E_{max} are shown as a function of $(t_s - t_o)$ in Figure 8 (by the dot-dashed, dashed and dotted lines, respectively). The solid line is the variation of E_{ic}. For steady state reconnection the $(t_s - t_o)$ axis could be replaced by a $(-t_s)$ axis for an equatorward moving satellite. This is thus an analytically calculated version of the schematic shown in Figure 2. The points A1 and B discussed in relation to Figure 2, are also marked. The bifurcation of the E_{min} curve is also shown, as in Figure 7, and the upper trace meets the E_{ic} curve at A1 (whereas the lower trace meets at A, at an energy $E_A < E_{A1}$). In either case, the rise and fall of V_{min}, as the field line evolves, can be seen to produce a highly characteristic feature in the spectrogram of low-altitude ion data. To investigate this further, Figure 9 shows the distribution functions $f(E)$ observed at low altitudes for the same $(t_s - t_o)$ as illustrated in figure 7. The general evolution predicted by using Figure 4 is observed at lower elapsed times since reconnection, but an isolated, spikelike feature also appears at low energies as the point $A1$ is approached (seen here in the case for $(t_s - t_o) = 520$ s).

In order to recognize this feature in data from a low-altitude ion detector, we must convolve these ideal spectra with the instrument response. Real data have limited time resolution (typically of $dt_s = 1$ s), are time averaged over an integration period of $\delta\tau$, and are aliased as the detector cycles around the energy channels within each dt_s. In addition, $f(E)$ are smoothed by the binning of data into various energy channels δE wide, and the detector will have limited pitch angle resolution. We here consider an instrument with two detectors, each with 10 energy channels which are addressed sequentially in order of descending energy, such that $\delta\tau = dt_s/10 = 0.1$ s. The energy resolution δE is $E/10$, and ions are detected over a 10° cone of pitch angles about zero. These characteristics are a simplified approximation of those of the ion instruments on board the DMSP satellites.

Figures 10 and 11 illustrate the effects of integration over the time $\delta\tau$ and coarse pitch angle and energy resolutions. *Lockwood and Davis* [1995a] have shown that time elapsed since reconnection $(t_s - t_o)$ has a range of the order of 550 s within a cusp which the satellite traversed in 78 s; in other

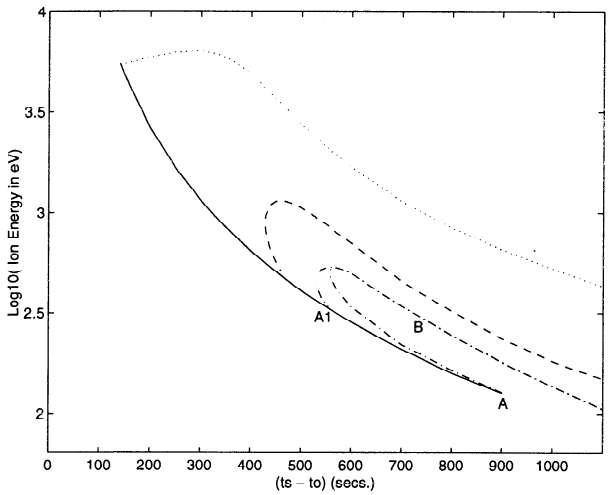

Figure 8. Features of a cleft/cusp/mantle ion plume spectrogram, shown on a logarithmic energy scale and as a function of time elapsed since reconnection $(t_s - t_o)$. The solid line is the low-energy cutoff energy, E_{ic}. As in Figure 7, the dot-dashed, dashed, and dotted lines show the variations of the minimum energy (E_{min}), the energy of peak distribution function (E_p), and the peak detected energy (E_{max}), respectively.

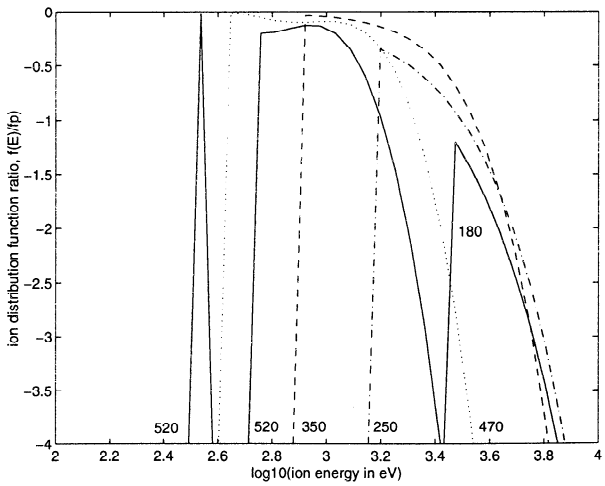

Figure 9. Distribution functions $f(E)$ of cusp ions in the topside ionosphere for various values of the elapsed time since reconnection of the observed field line $(t_s - t_o)$. These are termed ideal, since they do not allow for the limited time and energy resolution of a detector. The ratio of $f(E)$ to f_p, the peak f injected at the nose of the magnetosphere, is shown on a log-log scale.

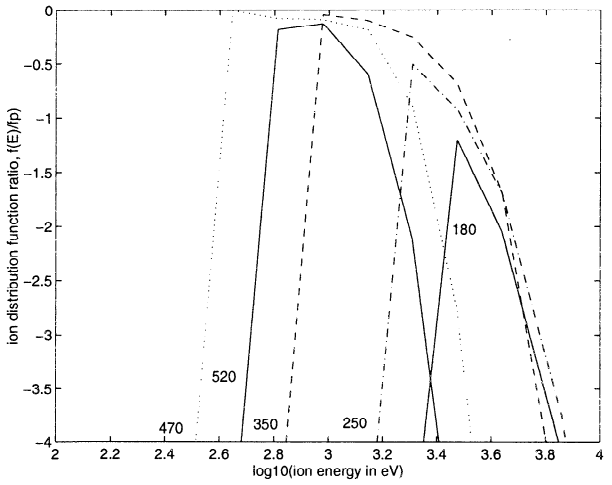

Figure 10. Averages of ideal spectra (of the kind shown in Figure 9) over 0.7-s ranges of elapsed time (t_s-t_o) and energy channels $\delta E = 0.1\ E$ wide, where the center energies, E are given in the text. Comparison with Figure 9 reveals the effects of time and energy averaging and coarse energy resolution.

words, $\Delta(t_s - t_o)/\Delta t_s = V_s/V_c \approx 550/78 \approx 7$. Hence data of time resolution $dt_s = 1$ s would typically cover greater than 7-s ranges of (t_s - t_o) in this case, and each integration period $\delta\tau$ covers 0.7 s of elapsed time since reconnection. However, if the reconnection rate were to be higher/lower than in the case studied by Lockwood and Davis, then the range of (t_s - t_o) in each $\delta\tau$ would be correspondingly lower/higher. In addition, we have to allow for a range of pitch angles, and thus a range of ion flight times. A larger pitch angle ion will have a somewhat longer flight time, and hence will have been injected somewhat earlier onto that field line, than a field-aligned ion seen simultaneously. The equations given by *Burch et al.* [1982] show that the flight time for nonzero pitch angle ions depends on the variation of the magnetic field, B, at all points along the field line between the injection point and the satellite. Thus the increase in flight time with pitch angle is not known without a full model of the field. To simulate the effect, we here consider that the detected ions are sufficiently close to being field aligned at the magnetopause that their $f(E)$ is independent of pitch angle. The range of ion flight times caused by the range of pitch angles can then be simulated by considering field-aligned ions for a range of (t_s - t_o). Figure 10 shows such averaged spectra, for 0.7-s ranges of (t_s - t_o), corresponding to the ideal spectra shown in Figure 9, but includes the effects of coarse energy resolution of the detector, for logarithmically spaced channels centered on the energies E with $\delta E/E$ of 0.1. The channels shown have E of 66, 97, 142, 207, 303 444, 649, 1390, 2030, 4350, 7240 and 9330 eV. The spikelike feature now only appears as a small ridge on the low-energy edge of the spectrum (for 470 s after reconnection) mainly because of the coarse sampling of energies.

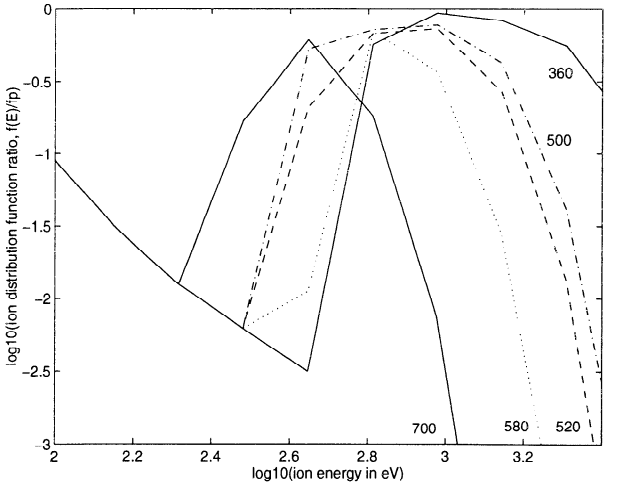

Figure 11. Detail of the evolution of the cut off in $f(E)$ with (t_s-t_o), allowing for both time and pitch angle averaging and for coarse energy bins, centered on the energies given the text.

In Figure 11, additional smoothing due to pitch angle effects are simulated by averaging over ranges of (t_s - t_o) to allow for larger pitch angle ions having a larger flight time. In other words, smoothing is caused by the range of magnetopause locations which contribute to the ions seen at any one t_s because more than one pitch angle is detected. Figure 11 shows the evolution of the f(E) cut-off in greater detail with this additional smoothing with $\Delta(t_s - t_o)/\Delta t_s = 60$. The point A is at an energy $E_A = m\ V_{fX}^2/2 = 142$ eV ($\log_{10}(E_A) = 2.15$, corresponding to the X line outflow speed of $V_{fX} = 165$ km s^{-1}), whereas the point A1, above which the ions travel adiabatically to the ionosphere without a second encounter with the magnetopause, is at $E_{A1} = 316$ eV ($\log_{10}(E_{A1}) = 2.5$, corresponding to 246 km s^{-1}). It can be seen that the point A1 is close to (but at an energy slightly below) where the ridge near the cut-off disappears completely in the averaged spectra.

Determination of E_{A1} from such $f(E)$ plots would thus contain large uncertainties. *Lockwood et al.* [1994] have noted that the identification of A1 is also possible from plots of the time series of distribution function seen in each energy channel. Distribution function f is usually presented as a function of velocity v, or energy E, at a given observation time, t_s, and thus denoted as $f(v)$ or $f(E)$, respectively; therefore $f(t_s)$ is here adopted as the notation for f as a function of t_s at constant v (and thus constant E). For this equatorward moving satellite, $f(t_s)$ falls as the satellite emerges through the equatorward edge of the cusp. Figure 12 shows $f(t_s)$ corresponding to the spectra shown in Figure 11; note that the decay happens earlier at lower energies, as predicted from Figure 2. The feature is clearly detectable as a secondary peak in the decay for the $E = 444$eV channel. ue to the field line acceleration effect, the channel closest to the actual value of E_A does not detect the secondary peak. From figures 11 and 12 we would deduce that a best estimate of E_{A1} of 303 eV, corresponding to a speed of 241 km s^{-1}, which is very close to the actual value (246 km s^{-1}) but 76 km s^{-1} larger than the true V_{fX} of 165 km s^{-1}. In this case, the model inputs were chosen to accentuate the difference between A and A1 and in general we would expect $(E_{A1}/2m)^{1/2}$ to be a less dramatic overestimate of V_{fX}. Work is underway to quantify this effect. The example presented here stresses the need for caution in trying to identify the point A and hence determine the speed V_{fX}. In summary, by using a combination of $f(E)$ and $f(t_s)$, the point A can be approximately ident-

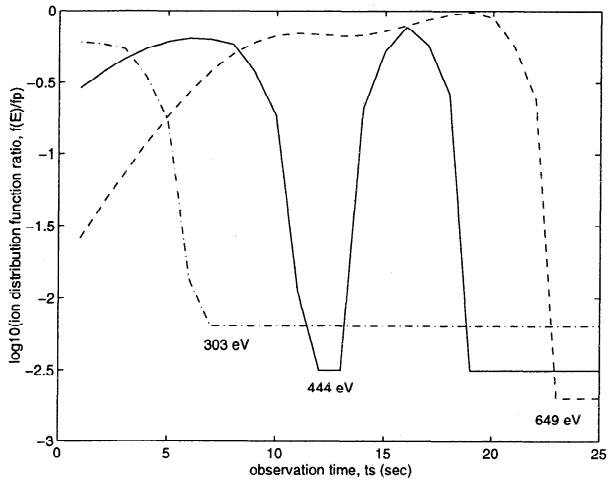

Figure 12. Modeled variations of $f(t_s)$ from the spectra shown in Figure 11, for three of the logarithmically spaced energy channels centered on the energies (E) given. In all cases, the decay of f from its peak value is shown as the satellite emerges through the equatorward edge of the cusp/cleft precipitation when $E = E_{ic}$.

ified, and V_{fX} can be determined. However, because of the field line acceleration, $E_{A1} > E_A$ and the technique will tend to overestimate V_{fX}.

The feature predicted here in $f(t_s)$ and $f(E)$ is unique to the reconnection model. Indeed, it only arises for field lines which accelerate over a sufficient distance of the magnetopause before straightening. To derive an order-of-magnitude estimate of the distance required, we note that for the feature to be clear, the minimum energy must rise by at least two instrument energy channels somewhere between $A1$ and B: for the case shown, the energy of A1 is E_{A1} = 303 eV and for the model ion detector described here, this requires E_{min} to rise to at least 700 eV (so no ions are seen in the channel centered on 649 eV), corresponding to V_{min} of 367 km s^{-1}: equation (3) shows that in general V_F will need to increase to more than this, because θ will increase to greater than zero (because the field line has straightened). If we assume a typical (and constant) field line acceleration of 1 km s^{-2} [*Lockwood and Smith*, 1994], this calls for the field line to move at least 7.5 R_E before it straightens. Hence the feature near A1 requires reconnection at quite low magnetic latitudes. Reconnection near the local cusp would not give this feature, but this may be only one of several reasons why it could be absent in data. Chief among these would be the characteristics of the detector, particularly if the energy, pitch angle, or time resolution is poor and the reconnection rate low. On the other hand, if the reconnection takes place at a site well beyond the flow stagnation point, V_f will initially be very low as the newly opened field lines contract under the curvature force against the magnetosheath flow. Later, V_f may rise to great values if the field line convects through the stagnation region toward the local magnetic cusp. *Lockwood* [1995b] has shown that such cases can accentuate the feature described here to such an extent that the cusp dispersion appears as a "double injection."

6. Variation of the Reconnection Rate and Location of the Reconnection Site

Lockwood and Smith [1994] have shown how large changes in the reconnection rate will cause changes in the variation of the elapsed time since reconnection (t_s - t_o) with the observation time t_s, giving subtle changes in the variation of E_{ic} with t_s. They estimated that $E_{ic}(t_s)$ would not be distinguishable from a steady state case unless the reconnection rate varies by a factor of at least 2. The effects of pulsed reconnection are clearest in the special case when the reconnection rate falls to zero between the pulses, giving discontinuous steps in $E_{ic}(t_s)$, as predicted by *Cowley et al.* [1991] and *Smith et al.* [1992] and employed in the interpretation of observed cusp ion steps by *Lockwood and Smith* [1992], *Escoubet et al.* [1992], and *Lockwood et al.* [1993a].

The equations derived by *Lockwood and Smith* [1992] can be applied to observed $E_{ic}(t_s)$. Specifically, the reconnection rate at the magnetopause X line is given by

$$\epsilon_y(t_o) = B_i(V_c\text{-}V_s)(dy/dy').\{1 + (d_o/2)(m/2)^{1/2} E_{ic}^{-3/2} dE_{ic}/dt_s\}^{-1} \quad (7)$$

where B_i is the ionospheric magnetic field, (dy/dy′) is the one-dimensional magnetic field mapping factor (dy is an element of length along the magnetopause X line and dy' is the corresponding length along the ionospheric merging gap), and V_s, V_c, d_o, m, and E_{ic} are as defined above. This equation is more general than that given by *Lockwood and Smith* [1992] because they assumed $|V_s| >> |V_c|$. Equation (7), on the other hand, can be applied to low-altitude satellites which move quasi-longitudinally, giving $V_s < V_c$. Such passes will show the sorts of $E_{ic}(t_s)$ variations discussed for mid-altitudes by *Lockwood and Smith* [1994]. The reconnection rate calculated by (7) is for a time t_o, given by equation (1) for $d_n = d_o$, $t_n = 0$ and $E_n = E_{ic}$.

The value of ϵ_y derived depends sensitively on the temporal gradient of E_{ic}. As pointed out by *Lockwood and Smith* [1992], the measurement errors are larger when the reconnection rate is large. To understand this, note that when the real ϵ_y is large and positive, $|dE_{ic}/dt_s|$ is small. A small error in the experimental determination in this gradient can then cause the estimated ϵ_y to be infinite (if the denominator in (7) goes to zero) or even negative. However, if ϵ_y is small, dE_{ic}/dt_s is large, and errors in its experimental estimation have little effect on the estimated ϵ_y. Another feature to note about equation (7) is that the value of ϵ_y does not only depend on dE_{ic}/dt_s, but this term is multiplied by a factor $E_{ic}^{-3/2}$. Hence periods of low ϵ_y give steep gradients in the cutoff energy E_{ic} when E_{ic} is large, but much less obvious gradients when E_{ic} is low. Hence, although inspection of cusp ion steps in any series of estimates of E_{ic} (as used by *Lockwood et al.* [1993a] and *Newell and Meng* [1995]) will reveal periods of low reconnection rate, the full duration of those low-rate periods is not determined unless equations (1) and (7) are used to compute $\epsilon_y(t_o)$.

Lockwood et al. [1993a] compared estimates of the intervals between reconnection pulses, taken from the size of cusp ion steps, with the European Incoherent Scatter (EISCAT) observations of the intervals between the associated poleward moving events. This comparison enabled them to estimate the distance d_o from the X line to the satellite. As discussed above, however, the full duration of the intervals

of low reconnection between the pulses is not estimated unless the variation $\epsilon_y(t_o)$ is calculated by using equation (7). Using only the steepest part of a step in E_{ic} would lead to an overestimate d_o as well as an underestimate of the period of low reconnection rate. These errors can be avoided by iterating d_o until the $\epsilon_y(t_o)$ from (7) matches the sequence of events seen from the ground.

Hence for the determination of both $\epsilon_y(t_o)$ and d_o, the accuracy with which the gradient dE_{ic}/dt_s is estimated is vital. *Lockwood and Smith* [1992] and *Newell and Meng* [1995] have both attempted to define an E_{ic} value for each spectrum (i.e., at each t_s) and then compared successive values. The problem with this approach is that each E_{ic} value has an error of at least plus or minus half the energy separation of the detector channels, making errors in the gradient (and hence also those in ϵ_y and d_o) large. *Lockwood and Smith* [1992] calculated these uncertainties in ϵ_y, arising from the coarse energy resolution of the detector, and they were very large indeed (even infinite) when the reconnection rate was high. However, by using the time series of distribution function, $f(t_s)$, the cutoff energy E_{ic} is accurately known at those t_s where it becomes equal to the energies of the detector channels (in the example used here of an equatorward moving satellite during southward IMF, this is when $f(t_s)$ decays). The times when this happens can be determined with much greater accuracy (plus or minus half of one time step), and the errors in ϵ_y are much smaller, although fewer data points are obtained [*Lockwood and Davis*, 1995b]. Furthermore, to derive a cutoff from a spectrum, either in distribution function $f(E)$ or differential energy flux $J_E(E)$, requires detection of a deviation from an assumed form (e.g., a drifting Maxwellian) which does not generally apply at low altitudes (because time-of-flight effects reveal a range of source locations and the injected ion spectrum varies with position along the magnetopause). No such assumption is required in looking for a decay in $f(t_s)$. *Lockwood and Davis* [1995b] have tested this procedure using simulated cusp ion data, and shown that the estimated reconnection rate is always correct to within the predicted uncertainties, which are relatively small.

7. Conditions at the Reconnection Site

As explained in section (4), ions injected in the immediate vicinity of the X line form the low-energy ion cutoff, $E_{ic}(t_s)$, in the ion spectrogram detected by a low-altitude satellite, for locations equatorward of A in Figure 2. For adiabatic scatter-free motion, both the energy E_{ic} and, by Liouville's theorem, $f(E_{ic})$ will be conserved on traveling from the X line to the satellite. Hence, by taking the values of $f(E_{ic})$ at various observation times, t_s, we can reconstruct the field-parallel part of the Cowley D distribution injected near the X line. A similar technique has recently been applied by *Elphic et al.* [1995] to dispersed ions in the plasma sheet boundary layer of the tail. Comparison of ideal data (like Figure 9) with time-aliased and energy-averaged simulations (like Figures 10, 11 and 12) shows that $f(E_{ic})$ and E_{ic} are best estimated as the last data point before $f(t_s)$ starts to fall as the satellite emerges through the equatorward edge of the cusp. This has been confirmed by using simulated $f(t_s)$ variations for a variety of steady and time-varying reconnection rates and solar wind conditions [*Lockwood and Davis*, 1995b]. This procedure is similar to the procedure adopted by *Hill and Reiff* [1977], but significantly different because they applied it to the peaks of the spectrum seen at each t_s, whereas we require the lower cutoff: As shown by Figures 4 and 9, these are only the same thing at high energies and can be considerably different at lower energies. This procedure has also been employed recently by *Lockwood et al.* [1994]. By fitting this derived Cowley D distribution in the LLBL with a drifting Maxwellian, we can find the bulk flow velocity, V_{pX}, the "field-parallel" density N' [see *Hill and Reiff*, 1977] and field-parallel temperature T of the ion distribution injected into the LLBL in the immediate vicinity of the X line.

The model of the cusp spectra and variations of $f(t_s)$ presented in section (4) allows us to approximately identify the point A which is at an energy $m(V_{fX})^2/2$, and hence to calculate the speed with which newly opened field lines emerge from the X line, V_{fX}. Near the X line we can take, to a very good approximation, $\cos \phi = \cos \theta = 1$. Hence from (4) we can compute the Alfvén speed at the X line to be

$$V_{AX} = V_{pX} - V_{fX} . \quad (8)$$

In addition, from (5) we find the component of the boundary-tangential sheath flow, in the plane of the sheath field, at the X line to be

$$V_{shX} = 2V_{fX} - V_{pX} \quad (9)$$

As discussind in section 4, the field line acceleration effect will tend to cause this V_{fX} estimate to be too large, and thus V_{shX} will tend to be overestimated and V_{AX} will tend to be underestimated.

Other useful information about the location and characteristics of the X line could be derived with knowledge of the spatial distribution of the magnetosheath ion density, $N_{sh}(d)$, the field-parallel ion temperature, $T_{sh}(d)$, and the magnetic field $B_{sh}(d)$, either from direct measurements or from interplanetary measurements, used in conjunction with a gas-dynamic sheath model. *Cowley* [1982] assumed that 50% of the incident magnetosheath ion population was transmitted through the RD (i.e., $t_r = N/N_{sh} = 0.5$) and 50% was reflected back into the magnetosheath. This value is a rough accord with the values of t_r determined experimentally by *Fuselier et al.* [1991], although other studies have implied that this factor may be lower [*Onsager et al.*, 1995; *Lockwood et al.*, 1994].

From the drifting Maxwellian fit to the transmitted Cowley D distribution, the values of the parallel ion temperature T and of the "one-dimensional" density $N' = (N/A) = (t_r N_{sh}/A)$ are known in the LLBL, where A is the temperature anisotropy of the ion gas distribution [see *Hill and Reiff*, 1977]. The magnetosheath field at the X line is given by

$$B_{sHX} = V_{AX} (\mu_o m N_{shX})^{0.5} = V_{AX} (\mu_o m N' A / t_r)^{0.5} \quad (10)$$

We can also apply conservation of mass and energy to the X line. The inflow energy is dominated by the Poynting flux (from both the magnetosheath and magnetosphere) which equals $\epsilon_y L(B_{sp}' + B_{sh}')/\mu_o$ for a length L of the magnetopause normal to the X line. This can be equated with the gain in the kinetic energy associated with the outflow plasma, which is $(dm/dt)V_{fX}^2/2$. By conservation of mass (dm/dt), the rate of mass transfer into the outflow region, is equal to

$m\epsilon_y L[(N_{sh}/B_{sh}') + (N_{sp}/B_{sp}')]$, the rate of mass flow in the inflow region; substituting yields

$$B_{sp}' + B_{sh}' = (V_{fX}^2\ m\ \mu_o/2)\ [(N_{sh}/B_{sh}') + (N_{sp}/B_{sp}')] \quad (11)$$

where B_{sp}' and B_{sh}' are the components of the magnetosphere and magnetosheath magnetic fields normal to the X line and N_{spX} and N_{shX} are the corresponding plasma densities in the magnetospheric and magnetosheath inflow regions. Because $N_{sp} << N_{sh}$ and B_{sp}' is generally greater than B_{sh}', we can neglect the (N_{sp}/B_{sp}') term in (11) to a first-order approximation. This yields a quadratic equation for B_{sh}', taking the positive solution for which yields the transverse magnetic shear across the X line;

$$\Delta B = B_{sh}' + B_{sp}' = -(B_{sp}'/2) + [(B_{sp}'^2/4) + (V_{fX}^2\ m\ \mu_o\ N_{sh}/2)]^{1/2} \quad (12)$$

In addition equation (11), with $(N_{sp}/B_{sp}') << (N_{sh}/B_{sh}')$, yields an expression for the outflow velocity:

$$V_{fX} = V_{AX} \cos\ \alpha\ (2 + 2B_{sp}'/B_{sh}')^{1/2} \quad (13)$$

where α is the angle that the magnetosheath field at the X line makes with the normal to the X line in the plane of the magnetopause, i.e., $\alpha = \cos^{-1}(B_{sh}'/B_{sh})$.

It is not possible to solve this set of equations, because there are too many unknowns like t_r, A, α, and T/T_{sh}. However, there are some constraints. For example $t_r \le 1$, $A \ge 1$, and $T/T_{sh} \ge 1$. In addition, a given value of A set limits to the decrease in N_{sh}, relative to values from the gasdynamic model, in the plasma depletion layer [see *Hill and Reiff*, 1977]. From the measured values of T and N we can place minimum values on both T_{sh} and N_{sh} which may limit how far from the nose of the magnetosphere the reconnection site must be.

Lockwood et al. [1994] have used these equations, along with simultaneous satellite data from the cusp and from the interplanetary medium, to investigate the magnetic shear across the X line and the transmission factor, t_r, for a "quasi-steady" cusp pass. Their analysis assumes that the dayside magnetopause is in quasi-equilibrium and uses the pressure balance equation in order to relate the observed solar wind dynamic pressure to the internal magnetospheric field, B_{sp}. Paper 2 [*Lockwood et al.*, this issue] applies the equations to a highly stepped cusp pass during which poleward moving events were seen by ground-based radars in very close conjunction to the satellite.

Acknowledgements. The author is grateful to M. P. Freeman, T. G. Onsager, M. F. Smith, D. Hardy, W. F. Denig, and S. W. H. Cowley for discussions relevant to this work, which was supported by the UK Particle Physics and Astronomy Research Council.

The Editor thanks P. T. Newell and another referee for their assistance in evaluating this paper.

References

Aggson, T. L., P. J. Gambardella, and N. C. Maynard, Electric field measurements at the magnetopause, 1, Observations of large convective velocities at rotational magnetopause discontinuities, *J. Geophys. Res., 88,* 10,000-10,010, 1983.

Biernat, H. K., M. Heyn, R. P. Rijnbeek, V. S. Semenov, and C. J. Farrugia, The structure of reconnection layers: Application to the Earth's magnetopause, *J. Geophys. Res., 94*, 287-298, 1989.

Burch, J. L., P.H. Reiff, R. A. Heelis, J. D. Winningham, W. B. Hanson, C. Gurgiolo, J. D. Menietti, R. A. Hoffman, and J. N. Barfield, Plasma injection and transport in the mid-altitude polar cusp, *Geophys. Res. Lett., 9,* 921-924, 1982.

Cowley, S. W. H., The causes of convection in the Earth's magnetosphere: A review of developments during the IMS, *Rev. Geophys., 20*, 531-565, 1982.

Cowley, S. W. H. and C. J. Owen, A simple illustrative model of open flux tube motion over the dayside magnetopause, *Planet. Space Sci., 37,* 1461, 1989.

Cowley, S. W. H., M. P. Freeman, M. Lockwood and M. F. Smith, The ionospheric signature of flux transfer events, in CLUSTER Dayside Polar Cusp, *Spec. Publ., ESA SP-330*, edited by C. I. Barron, pp. 105-112, Eur. Space Agency Publ., Netherlands, 1991.

Crooker, N. U., Dayside merging and cusp geometry, *J. Geophys. Res., 84*, 951-959, 1979.

de Hoffmann, F., and E. Teller, Magneto-hydrodynamic shocks, *Phys. Rev., 80*, 692, 1950.

Elphic, R. C., T.G. Onsager, M.F. Thomsen and J.T. Gosling, Nature and location of the source of the plasma sheet boundary layer ion beams, *J. Geophys. Res., 100,* 1857-1870, 1995.

Escoubet, C. P., M. F. Smith, S. F. Fung, P. C. Anderson, R. A. Hoffman, E. M. Basinska, and J. M. Bosqued, Staircase ion signature in the polar cusp: A case study, *Geophys. Res. Lett., 19,* 1735-1738, 1992.

Fedder, J. A., C. M. Mobarry, and J. G. Lyon, Reconnection voltage as a function of IMF clock angle, *Geophys. Res. Lett., 18,* 1047-1050, 1991.

Frank, L. A., Plasmas in the Earth's polar magnetosphere, *J. Geophys. Res., 76,* 5202-5219, 1971.

Fuselier, S. A., D. M. Klumpar, and E. G. Shelley, Ion reflection and transmission during reconnection at the Earth's subsolar magnetopause, *Geophys. Res. Lett., 18,* 139-142, 1991

Gosling, J. T., M. F. Thomsen, S. J. Bame, R. C. Elphic, and C. T. Russell, Plasma flow reversals at the dayside magnetopause and the origin of asymmetric polar cap convection, *J. Geophys. Res., 95,* 8073-8084, 1990a.

Gosling, J. T., M. F. Thomsen, S. J. Bame, R. C. Elphic and C. T. Russell, Cold ion beams in the low-latitude boundary layer during accelerated flow events, *Geophys. Res. Lett., 17,* 2245-2248, 1990b.

Gosling, J. T, M. F. Thomsen, S. J. Bame, R. C. Elphic, and C. T. Russell, Observations of reconnection of interplanetary and lobe magnetic field lines at the latitude magnetopause., *J. Geophys. Res., 96,* 14,097-14,106, 1991.

Heikkila, W. J., and J. D. Winningham, Penetration of magneto sheath plasma to low altitudes through the dayside magnetospheric cusps, *J. Geophys. Res., 76,* 883-891, 1971.

Hill, T. W., Rates of mass, momentum, and energy transfer at the magnetopause, in *Proceedings of the Magnetospheric Boundary Layers Conference, Alpbach, Spec. Publ., SP-148*, pp. 325-333, Eur. Space Agency, Neuilly, France, 1979.

Hill, T. W., and P. H. Reiff, Evidence of magnetospheric cusp proton acceleration by magnetic merging at the dayside magnetopause, *J. Geophys. Res., 82,* 3623-3628, 1977.

Hudson, P. D., Discontinuities in an isotropic plasma and their identification in the solar wind, *Planet. Space Sci., 18,* 1611-1622, 1970.

Johnstone, A. D., D. J. Rodgers, A. J. Coates, M. F. Smith, and D. J. Southwood, Ion acceleration during steady state reconnection at the dayside magnetopause, in *Ion Acceleration in the Magnetosphere and Ionosphere*, edited by T. Chang et al., *Geophys. Monogr. Ser., vol.* 38, pp. 136-145, AGU, Washington, D. C., 1986.

Lin, Y., and L.C. Lee, Structure of the dayside reconnection layer in resistive MHD and hybrid models, *J. Geophys. Res., 98,* 3919-3934, 1993.

Lockwood, M., Ionospheric signatures of pulsed magnetopause reconnection in *Physical Signatures of Magnetopause Boundary*

Layer Processes, NATO ASI Ser. C, vol. 425, ed. J. Holtet and A. Egeland, pp. 229-243, Kluwer, Acad. Norwell Mass., 1994.

Lockwood, M., Ground-based and satellite observations of the cusp: Evidence for pulsed magnetopause reconnection, in *Physics of the Magnetopause, Geophys. Monogr., Ser.*, edited by P. Song and B. U. O. Sonnerup, AGU, Washington, D. C., in press, 1995a.

Lockwood, M., Overlapping cusp ion injections: An explanation invoking magnetopause reconnection, *Geophys. Res. Lett., 22,* 1141-1144, 1995b.

Lockwood, M., and C. J. Davis, The occurrence probability, width, and number of steps of cusp precipitation for fully pulsed reconnection at the dayside magnetopause, *J. Geophys. Res., 100,* 7627-7640, 1995a.

Lockwood, M., and C. J. Davis, An analysis of the accuracy of magnetopause reconnection rate variations deduced from cusp ion dispersion characteristics, *Ann. Geophys.*, in press, 1995b.

Lockwood, M., and M. F. Smith, Low-altitude signatures of the cusp and flux transfer events, *Geophys. Res. Lett., 16,* 879-882, 1989.

Lockwood, M., and M. F. Smith, The variation of reconnection rate at the dayside magnetopause and cusp ion precipitation, *J. Geophys. Res., 97,* 14,841-14,847, 1992.

Lockwood, M., and M. F. Smith, Comment on "Mapping the dayside ionosphere to the magnetosphere according to particle precipitation characteristics" by Newell and Meng, *Geophys. Res. Lett., 20,* 1739, 1993.

Lockwood, M., and M. F. Smith, Low and middle altitude cusp particle signatures for general magnetopause reconnection rate variations, 1, Theory, *J. Geophys. Res., 99,* 8531-8533, 1994.

Lockwood, M., W. F. Denig, A. D. Farmer, V. N. Davda, S. W. H. Cowley, and H. Lühr, Ionospheric signatures of pulsed magnetic reconnection at the Earth's magnetopause, *Nature, 361*(6411), 424, 1993a.

Lockwood, M., J. Moen, S. W. H. Cowley, A. D. Farmer, U. P. Løvhaug, H. Lühr, and V. N. Davda, Variability of dayside convection and motions of the cusp/cleft aurora, *Geophys. Res. Lett., 20,* 1011-1014, 1993b.

Lockwood, M., T. G. Onsager, C. J. Davis, M. F. Smith and W. F Denig, The characteristics of the magnetopause reconnection X line deduced from low-altitude satellite observations of cusp ions, *Geophys. Res. Lett., 21,* 2757-2760, 1994.

Lockwood, M., C. J. Davis, M. F. Smith, T. G. Onsager, and W. F Denig, Location and characteristics of the reconnection X line deduced from low-altitude satellite and ground-based observations, 2, DMSP and EISCAT data, *J. Geophys. Res.*, this issue.

Newell, P. T., and C.-I. Meng, The cusp and the cleft/boundary layer: Low-altitude identification and statistical local time variation, *J. Geophys. Res., 93,* 14,549-14,556, 1988.

Newell, P. T., and C. -I. Meng, Magnetopause dynamics as inferred from plasma observations on low-altitude satellites, in *Physics of the Magnetopause*, edited by B. U. O Sonnerup, AGU, Washington, D. C., *Geophys. Monogr. Ser.*, in press, 1995.

Newell, P. T., W. J. Burke, C. -I. Meng, E. R. Sanchez, and M. E. Greenspan, Identification an observation of the plasma mantle at low altitude, *J. Geophys. Res., 96,* 35-45, 1991.

Onsager, T. G., A quantitative model of magnetosheath plasma in the low-latitude boundary layer, cusp and mantle, in *Physical Signatures of Magnetopause Boundary Layer Processes, NATO ASI Ser. C*, vol. 425, edited by J. A. Holtet and A. Egeland, pp. 385-400, Kluwer Acad., Norwell, Mass., 1994.

Onsager, T. G., and S. A. Fuselier, The location of the magnetopause reconnection for northward and southward interplanetary magnetic field, in *Solar System Plasmas in Space and Time, Geophys. Monogr. Ser.*, vol. 84, edited by J. L. Burch and J. H. Waite Jr., pp. 183-197, AGU, Washington D. C., 1994.

Onsager, T. G., C. A. Kletzing, J. B. Austin, and H. MacKiernan, Model of magnetosheath plasma in the magnetosphere: Cusp and mantle precipitations at low altitudes, *Geophys. Res. Lett., 20,* 479-482, 1993.

Onsager, T. G., et al., Low-altitude observations and modeling of quasi-steady magnetopause reconnection, *J. Geophys. Res., 100,* 11,831-11,843, 1995.

Paschmann, G., The Earth's magnetopause, in *Achievements of the International Magnetospheric Study, IMS, Spec Publ., ESA SP-217*, pp 53-64, Eur. Space Res. and Technol. Cent., Nordvijk, Netherlands, 1984.

Paschmann, G., B. U. Ö. Sonnerup, I. Papamastorakis, N. Sckopke, G. Haerendel, S. J. Bame, J. R. Asbridge, J. T. Gosling, C. T. Russell, and R. C. Elphic, Plasma acceleration at the Earth's magnetopause: Evidence for reconnection, *Nature, 282,* 243-246, 1979.

Paschmann, G., I. Papamastorakis, W. Baumjohann, N. Sckopke, C. W. Carlson, B. U. Ö. Sonnerup, and H. Lühr, The magnetopause for large magnetic shear: AMPTE/IRM observations, *J. Geophys. Res., 91,* 11,099-11,115, 1986.

Paschmann, G., B. U. Ö. Sonnerup, I. Papamastorakis, W. Baumjohann, N. Sckopke, and H. Lühr, The magnetopause and boundary layer for small magnetic shear: Convection electric fields and reconnection, *Geophys. Res. Lett., 17,* 1829-1832, 1990.

Phillips, J. L., S. J. Bame, R. C. Elphic, J. T. Gosling, M. F. Thomsen and T. G. Onsager, Well-resolved observations by ISEE 2 of ion dispersion in the magnetospheric cusp, *J. Geophys. Res., 98,* 13,429-13,440, 1993.

Reiff, P. H., T. W. Hill, and J. L. Burch, Solar wind plasma injection at the dayside magnetospheric cusp, *J. Geophys. Res., 82,* 479-491, 1977.

Rosenbauer, H., H. Gruenwaldt, M. D. Montgomery, G. Paschmann and N. Sckopke, HEOS 2 plasma observations in the distant polar magnetosphere: The plasma mantle, *J. Geophys. Res., 80,* 2723-2737, 1975.

Sanchez, E. R. and G. L. Siscoe, IMP 8 magnetotail boundary crossings: a test of the MHD models for an open magnetosphere, *J. Geophys. Res., 95,* 20,771-20,779, 1990.

Sanchez, E. R., G. L. Siscoe, J. T. Gosling, E. W. Hones Jr., and R. P. Lepping, Observations of rotational discontinuity-slow mode expansion fan structure of the magnetotail boundary, *J. Geophys. Res., 95,* 61-73, 1990.

Shelley, E. G., R. D. Sharp, and R.G. Johnstone, He^{++} and H^{+} flux measurements in the dayside cusp: Estimates of convection electric field, *J. Geophys. Res., 81,* 2363-2370, 1976.

Smith, M. F., and D. J. Rodgers, Ion distributions at the dayside magnetopause, *J. Geophys. Res., 96,* 11,617-11,624, 1991.

Smith, M. F., M. Lockwood, and S. W. H. Cowley, The statistical cusp: A simple flux transfer event model, *Planet. Space Sci., 40,* 1251, 1992.

Sonnerup, B. U. O., G. Paschmann, I. Papamastorakis, N. Sckopke, G. Haerendel, S.J. Bame, J.R. Ashbridge, J.T. Gosling, and C.T. Russell, Evidence for magnetic field reconnection at the Earth's magnetopause, *J. Geophys. Res., 86,* 10,049-10,067, 1981.

Sonnerup, B. U. Ö., I. Papamastorakis, G. Paschmann, and H. Lühr, The magnetopause for large magnetic shear: Analysis of convection electric fields from AMPTE/IRM, *J. Geophys. Res., 95,* 10,541-10,557, 1990.

Spreiter, J.R. A.L. Summers and A.Y. Alksne, Hydromagnetic flow around the magnetosphere, *Planet. Space Sci., 14,* 223-253, 1966.

M. Lockwood, Rutherford Appleton Laboratory, Chilton, Didcot, OX11 0QX, United Kingdom. (e-mail: Internet. mike@eiscat.ag.rl.ac.uk)

(Received November 28, 1994; revised April 25, 1995; accepted April 25, 1995.)